Normal Modes of the Atmosphere as Estimated by Principal Oscillation Patterns and Derived from Quasigeostrophic Theory

REINER SCHNUR

Max-Planck-Institut für Meteorologie, Hamburg, Germany

GERHARD SCHMITZ AND NORBERT GRIEGER

Institut für Atmosphärenphysik, Kühlungsborn, Germany

HANS VON STORCH

Max-Planck-Institut für Meteorologie, Hamburg, Germany

(Manuscript received 6 April 1992, in final form 19 October 1992)

ABSTRACT

The principal oscillation pattern (POP) analysis is a technique to empirically identify time-dependent spatial patterns in a multivariate time series of geophysical or other data. In order to investigate medium-scale and synoptic waves in the atmosphere it has been applied to tropospheric geopotential height fields of ECMWF analyses from 1984 to 1987. The data have been subjected to zonal Fourier decomposition and to time filtering so that variations with periods between 3 and 25 days were retained. Analyses have been performed separately for each zonal wavenumber 5–9 on the Northern Hemisphere in winter and on the Southern Hemisphere in summer (DJF).

POPs can be seen as normal modes of a linear approximation to a more complex dynamical system. The system matrix is estimated from observations of nature. This concept is compared with conventional stability analysis where the system matrix of the linear system is derived from theoretical, in this case quasigeostrophic, reasoning. Only the mean basic flow depends on time- and space-averaged fields of observed wind and temperature from the ECMWF data.

It turns out that the most significant POPs are very similar in time and spatial structure to the most unstable waves in the stability analysis. They describe the linear growth phase of baroclinic, unstable waves that propagate eastward with periods of 3–7 days. Since the POPs are purely derived from observations, the results indicate the appropriateness of the assumptions usually made in linear stability analysis of zonally symmetric flows to explain high-frequency atmospheric fluctuations.

Moreover, the POP analysis reveals patterns that are not found in the linear stability analysis. These can possibly be attributed to the nonlinear decay phase of baroclinic waves. Eliassen–Palm cross sections help clarify the interpretation of the POPs in terms of the life cycle of nonlinear baroclinic waves.

1. Introduction

Medium-scale and synoptic waves (zonal wavenumbers 4–9) are known to be responsible for much of the midlatitude atmospheric variability. In a series of papers, Fraedrich et al. (Fraedrich and Böttger 1978; Fraedrich and Kietzig 1983) applied space–time spectral analyses to observations of tropospheric variables at selected latitudes in order to investigate the frequency distribution of progressive and retrogressive disturbances. Wavenumber–frequency contours of the power spectrum density at 50°N for wintertime geopotential height (Fig. 1; the symbols will be discussed later) show, for instance, that variance maxima are connected with eastward-propagating waves of zonal wavenumbers 5–9, with periods between 3 and 10 days. The maxima are well separated from a secondary maximum in the region of retrogressive waves (shaded region in Fig. 1) and are of about the same amount as maxima of the stationary variance in similar plots (not shown). However, the retrogressive and stationary variance maxima are confined to the low-frequency band, with periods above 10 days, and to wavenumbers 1–4. They are not an issue in this paper.

Experiments with a hierarchy of models reaching from linear geostrophic to nonlinear primitive equation models with zonally symmetric or asymmetric flows in β channels or on a sphere (Charney 1947; Eady 1949; Simmons and Hoskins 1976; Frederiksen 1982) have been performed with the intention of investigating the processes that cause this maximum in space–time spectra. They lead to the insight that the high-frequency

Corresponding author address: Dr. Reiner Schnur, Max-Planck-Institut für Meteorologie, Bundesstrasse 55, D-2000 Hamburg 13, Germany.

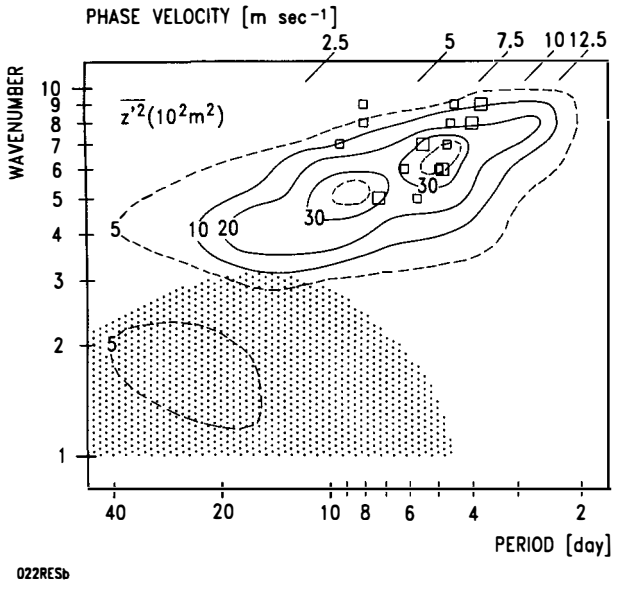

FIG. 1. Power spectrum of geopotential height at 500 mb and 50°N (one-sided frequency spectrum). Contours show the propagating variance (average of five winters 1972/73–1976/77), and the shaded region indicates westward progression. The symbols denote the periods of the POPs from the Northern Hemisphere POP analyses for zonal wavenumbers 5–9 (section 4). Big squares are for the POPs that explain most of the variance for each wavenumber. [Adapted from Fraedrich and Böttger (1978)].

characteristics of the circulation can be attributed to the generation of waves and cyclones as a result of the baroclinic instability of the mean climatological flow to small disturbances. The evolution of these perturbations is governed by wave–zonal mean energy exchanges and exhibits a well-defined life cycle of linear baroclinic growth, maturity, and nonlinear barotropic decay. The latter stage is also influenced by wave–wave interactions. Both statistical investigations and case studies (Randel and Stanford 1985a, 1985b; Blackmon et al. 1984a, 1984b; Lim and Wallace 1991) were able to track this behavior in observations. The eastward progression is a more global feature in the Southern Hemisphere than it is in the Northern Hemisphere, where the waves are often confined to local storm-track regions due to land–sea contrasts.

In the above-mentioned theoretical studies, the high-frequency atmospheric transient fluctuations are often seen as being the normal modes of a dynamical system that has been derived from more or less severe simplifications of the real world. The baroclinic linear stability analysis of zonally symmetric flows in a quasigeostrophic model has been especially historically useful in understanding midlatitude atmospheric circulation. Though nonlinearity and asymmetric basic states have been shown to contribute to the evolution of baroclinically unstable waves, it is still of importance because the relatively simple computations allow for a variety of experiments.

The purpose of this paper is to introduce the normal-mode concept to the class of observational studies in this context by using the principal oscillation pattern (POP) analysis (Hasselmann 1988). This technique computes the normal modes of a linear dynamical system on which noise is superimposed by considering a system matrix that is estimated from observations (von Storch et al. 1988). It is designed to empirically detect regularly oscillating patterns in multivariate time series and has so far been used in a number of studies that were primarily concerned with issues on longer time and space scales than is the case here (von Storch et al. 1990; Xu 1990; Xu 1993).

It will turn out that the POP analysis is a convenient method for extracting time-dependent patterns from observational data representing fluctuations in atmospheric circulation on the time and spatial scales discussed above. Moreover, by analyzing the observations in a way that is analogous to the way the theoretical dynamics are analyzed (normal modes) the comparison between observations and theory is facilitated.

The organization of this paper is as follows. In section 2, a theoretical outline of the normal-mode concept is given. Section 2a introduces the principal oscillation pattern technique in this context. The analysis of the stability of a flow with respect to small disturbances is sketched in section 2b. Section 3 describes the data used and the respective steps that have been performed in the analyses. In section 4 the results for the Northern (4a) and Southern hemispheres (4b) are presented in detail. All results are listed again in the Appendix in the form of two tables. Section 4 focuses on the comparison between the POPs and the baroclinic unstable waves in their linear growing phase. A connection between some additional POPs and the nonlinear barotropic decay phase of unstable waves is hypothesized. This is substantiated in section 5 by means of Eliassen–Palm cross sections. In section 6, the results are summarized and discussed, and some remaining tasks are given.

2. Analysis techniques: Normal modes

Let

$$\mathbf{X}(t+1) = \mathbf{A}\mathbf{X}(t) \tag{1}$$

be a discretized first-order linear Markov process in n-dimensional space. The state vector $\mathbf{X}$ may be expanded in terms of the *normal modes* of this process, which are the eigenvectors $\mathbf{P}$ of the system matrix $\mathbf{A}$. In most cases, these will form a complete set of n linearly independent vectors, so that $\mathbf{X}$ can be represented as a linear sum of the eigenvectors:

$$\mathbf{X}(t) = \sum z_j(t)\mathbf{P}_j. \tag{2}$$

The quantity $z_j(t)$ is called the coefficient time series of mode $\mathbf{P}_j$. Note that since the eigenvectors need not

to be orthogonal, the coefficients z_j depend on all modes and not only on $\mathbf{P}_j$.

In general, matrix $\mathbf{A}$ is not symmetric and some or all of its eigenvalues σ, eigenvectors $\mathbf{P}$, and coefficients z are complex. However, since $\mathbf{X}$ and $\mathbf{A}$ are real, all complex quantities appear in complex-conjugate pairs.

Equation (2) can be inserted into (1) yielding

$$z_j(t+1) = \sigma_j z_j(t), \tag{3}$$

which defines a damped ($|\sigma| < 1$) or growing ($|\sigma| > 1$) harmonic oscillation for the coefficient time series z_j, with a characteristic period $T_j = 2\pi/\omega_j$ and an *e*-folding time $\tau_j = -1/\ln|\sigma_j|$, derivable from the eigenvalue $\sigma_j = |\sigma_j| \exp(i\omega_j)$. It follows that, apart from the damping/growing, the dynamical evolution of the system described by one normal mode $\mathbf{P} = \mathbf{P}^1 + i\mathbf{P}^2$, with period T, can be visualized by the following infinite cyclic sequence:

$$\cdots \rightarrow \mathbf{P}^2 \rightarrow \mathbf{P}^1 \rightarrow -\mathbf{P}^2 \rightarrow -\mathbf{P}^1 \rightarrow \mathbf{P}^2 \rightarrow \cdots. \tag{4}$$

A transition between two patterns in (4) is performed in one quarter of a period $T/4$.

So far, all relationships are based on the existence of a dynamical system (1) with a system matrix $\mathbf{A}$. But, in most practical situations, what is lacking is exactly the knowledge of this matrix because the dynamics of the system of interest are not understood or are too complex. In the remainder of this section two different approaches of how to deal with this problem are described.

a. *Principal oscillation patterns*

The first approach for determining an appropriate system matrix is a statistical one. It is based on the idea that although the dynamics of a system may be unknown, there is perhaps a set of observations available that describes the history of the system's state in some variables of interest. If it is assumed that the dynamics of a part of the system are governed by a linear operator and that the role of those parts, which are not covered by this operator, is just to act as background noise (or forcing), the following basic ansatz is obtained:

$$\mathbf{X}(t+1) = \mathbf{A}\mathbf{X}(t) + \text{noise}. \tag{5}$$

Equation (5) describes a first-order autoregressive process (von Storch et al. 1988).

Let $\mathbf{X}$ be stationary with zero mean. If $\mathbf{X}$ and the noise are uncorrelated, then multiplication of (5) from the right-hand side by the transpose of $\mathbf{X}(t)$, and taking expectation, $\mathbf{E}$, leads to

$$\mathbf{A} = \mathbf{E}[\mathbf{X}(t+1)\mathbf{X}^{\mathrm{T}}(t)]\{\mathbf{E}[\mathbf{X}(t)\mathbf{X}^{\mathrm{T}}(t)]\}^{-1}, \tag{6}$$

which minimizes the noise term in (5) in the least-squares sense. Since the true expectations in (6) for the stochastic process $\mathbf{X}$ are unknown, the lag-0 and lag-1 covariance matrices have to be estimated from observational data.

The eigenvectors of (6), or the normal modes of (5), are called *principal oscillation patterns* (POPs). The time coefficients $z(t)$ are called *POP coefficients*. Their time evolution is given by (omitting the index)

$$z(t+1) = \sigma z(t) + \text{noise}, \tag{7}$$

which, in the absence of noise, defines a cycle (4) in terms of the real and imaginary part of a POP. Note that the stationarity of $\mathbf{X}$ requires $|\sigma| < 1$.

b. *Linear stability analysis*

Sometimes, the dominant mechanisms in a system are known, and the dynamical equations may be written as

$$\frac{\partial \mathbf{X}}{\partial t} = \mathbf{L}(\mathbf{X}) + \text{forcing terms}, \tag{8}$$

where $\mathbf{L}$ is some operator. However, often $\mathbf{L}$ will be nonlinear, and then (8) will be too complex to be solved analytically. A conventional approach to this difficulty is as follows.

If, say, in the absence of forcing, (8) has an exact steady-state solution $\mathbf{X}^s$, then the investigation of the evolution of the state $\mathbf{X}$ is equivalent to the study of its deviations $\mathbf{X}'(t)$ from $\mathbf{X}^s$. Thus, after discretization, (8) becomes an equation for $\mathbf{X}'$,

$$\mathbf{X}'(t+1) = \mathbf{L}^{\mathbf{X}^s}[\mathbf{X}'(t)], \tag{9}$$

with the operator $\mathbf{L}^{\mathbf{X}^s}$ depending on $\mathbf{X}^s$. If it is now assumed that the perturbations $\mathbf{X}'$ are initially small, then (9) may be linearized, neglecting all $\mathbf{X}'$ terms of order higher than one. What is obtained is the system equation (1) for the perturbation state $\mathbf{X}'$, with a matrix $\mathbf{A}$ depending on the basic state $\mathbf{X}^s$. The normal modes of this system may be computed as described above, and $\mathbf{X}'$ may be expanded as in (2). The vector of state may be restored by means of $\mathbf{X}(t) = \mathbf{X}^s + \mathbf{X}'(t)$.

The time evolution of each mode is given by (3). The normal modes with eigenvalues $|\sigma| > 1$ will grow in amplitude and will describe the instability of the basic state $\mathbf{X}^s$ to small perturbations. The computation of the normal modes for different perturbations and subsequent analysis of their growth rates is known as *linear stability analysis*. The most unstable modes will emerge first from a background of small disturbances and will, thus, describe the major part of the underlying processes. Note that this concept is only valid as long as the amplitudes of the perturbations are small and that after some time of growth, nonlinear processes can no longer be ignored.

The steady states $\mathbf{X}^s$ are often replaced by other basic states. Experimenting with different arbitrarily prescribed basic states may yield considerable insights into the dynamics of a system. In the atmospheric sciences

$\mathbf{X}^s$ is also often taken to be a climatological basic state that is derived from observations. In this paper, too, the stability of such an observed basic state is considered.

3. Data and analyses

The data used in this study are taken from the European Centre for Medium-Range Weather Forecasts (ECMWF) global analysis dataset, which consists of twice daily data for several atmospheric variables. The spatial resolution is 2.5° × 2.5° at the seven vertical levels 1000, 850, 700, 500, 300, 200, and 100 hPa. The time interval covered here is 1984–1987, during which the analyses are fairly stationary (cf. Trenberth and Olson 1988).

In an attempt to identify midlatitude baroclinic waves in the troposphere, a set of POP analyses and linear stability analyses have been performed on both hemispheres in northern winter, in the manner described in the following. Since the signals are expected to propagate mostly in the zonal direction on top of a zonally symmetric mean flow, a semispectral representation is used by means of zonal Fourier decomposition.

The variable analyzed with the POP method is the geopotential height Φ from the ECMWF data at the seven available levels. Since we are looking for high-frequency signals, all data were first band-pass filtered so that only the anomalies on time scales between 3 and 25 days were retained. Then, two datasets were formed: a Northern Hemisphere dataset (10°–85°N) and a Southern Hemisphere set (10°–85°S), both for the three northern winters (DJF) 1984/85–1986/87. These data were Fourier decomposed along each latitude using the standard scheme

$$\Phi(\lambda, \theta, p) = \sum_k c_k(\theta, p)\cos(k\lambda) + s_k(\theta, p)\sin(k\lambda), \tag{10}$$

where (λ, θ, p) denotes (longitude, latitude, pressure), and k represents zonal wavenumber. In this study, only wavenumbers 5–9 are considered. The state vector $\mathbf{X}_k$ was then formed for each of these wavenumbers by

$$\mathbf{X}_k = \begin{bmatrix} \vdots \\ c_k(\theta_i, p_j) \\ s_k(\theta_i, p_j) \\ \vdots \end{bmatrix}_{i,j}, \tag{11}$$

where θ_i and p_j denote the latitudes and pressure levels of the data grid ($k = 5, \cdots, 9$).

The "spatial" dimension of the system for the given resolution is, thus, (31 latitudes × 7 levels × 2 Fourier coefficients) = 434. Since no reduction of the dimension of the problem is incorporated into the POP method itself, the data were subjected to a truncated EOF (empirical orthogonal functions) expansion prior to the analysis. The time series of vectors (11) was EOF expanded, and the vector of only the first 18 EOF coefficients was used as new time series. This retained more than 95% of the total variance of the data. A positive by-product of this procedure is to exclude noisy components from the analysis. Having done a POP analysis, the patterns are immediately restored back from EOF space to physical space, so the representation (11) will always be used in this paper.

Since $\mathbf{X}$ is formed by the cosine and sine coefficients of zonal geopotential waves, both the real and the imaginary parts of a POP $\mathbf{P} = \mathbf{P}^1 + i\mathbf{P}^2$ must be interpreted as vectors of Fourier coefficients too. An amplitude–phase notation

$$c(\theta, z)\cos(k\lambda) + s(\theta, z)\sin(k\lambda) = A(\theta, z)\cos[k\lambda - \Xi(\theta, z)]$$

will be used to represent the patterns. Thus, $\mathbf{P}^1$ ($\mathbf{P}^2$) is represented by the latitude–height distribution of a phase Ξ^1 (Ξ^2) and an amplitude A^1 (A^2). If $\mathbf{P}^1$ and $\mathbf{P}^2$ are 90° out of phase (i.e., a quarter of a wavelength), and if the amplitudes are nearly equal, the two patterns represent a zonally propagating wave according to the transition cycle (4). For the limiting case that one part has very small amplitudes compared to the other part, the POP approximates a standing wave. Note that since the structures of Ξ^1 and Ξ^2, as well as A^1 and A^2, may differ, (4) allows for a change of shape of the wave during its evolution cycle or for meridionally or vertically meandering traveling waves.

The linear stability analysis has been set up to be as similar to the POP analysis as possible. The starting point is the quasigeostrophic approximation to the potential-vorticity equation for a stratified fluid on a hemisphere without topography that defines the operator $\mathbf{L}$ in (8). No forcing or dissipation is included. The model has been described in Charney and Stern (1962). Its vertical coordinate is geometric height, and the vertical extension of the model atmosphere is 0–16 km, corresponding to an equivalent height of about 1000 to 100 hPa (the highest level in the POP analyses).

The model equation is linearized about a zonally symmetric basic state, and the perturbation streamfunction Ψ' is expanded as in (10) for zonal wavenumbers k. Discretization on a model grid with 1-km vertical and 2° meridional resolution then leads to an equation (1) for each wavenumber and for the state vector $\mathbf{X}_k$ of cosine and sine coefficients

$$\mathbf{X}_k = \begin{bmatrix} \vdots \\ c_k(\theta_i, z_j) \\ s_k(\theta_i, z_j) \\ \vdots \end{bmatrix}_{i,j}, \tag{12}$$

where θ_i and z_j denote latitude and the geometric height of the model grid. The linear stability analysis then

consists of solving an eigenvalue–eigenvector equation for each wavenumber k = 5–9, as described in section 2b.

In this study, a climatological basic flow, as derived from ECMWF wind data from DJF 1984/85–1986/87, is used as $\mathbf{X}^s$. The static stability parameter in the vorticity equation depends on the vertical profile of horizontally averaged temperature. This is again taken from the ECMWF data as the mean over the same three winters for which the POP analyses were carried out and interpolated to the model grid. On the upper and lower boundary, a zero vertical perturbation wind is prescribed. The model is formulated for each hemisphere, with the boundary condition of zero streamfunction at the equator and at the poles.

The zonal waves corresponding to the most unstable modes $\mathbf{Q} = \mathbf{Q}^1 + i\mathbf{Q}^2$ will be considered. As described above, $\mathbf{Q}^1$ and $\mathbf{Q}^2$ can be represented in an amplitude–phase notation and evolve according to cycle (4). However, since the system matrix **A** only depends on a zonally averaged basic state, the normal modes must be invariant against zonal displacements. Therefore, $\mathbf{Q}^1$ and $\mathbf{Q}^2$ coincide, except for a phase difference of 90°, so that **Q** represents a pure, zonally propagating pattern. This was not the case in the POP analysis, since the matrix **A** was of general form, and the observation data satisfy, of course, no such invariance condition.

Note that the above-described formulation of the stability problem is equivalent to the usual use of the perturbation streamfunction

$$\mathbf{X}'(\lambda, \theta, z, t) = \mathrm{Re}[\hat{\mathbf{X}}_k(\theta, z) \exp(ik\lambda - i\omega t)],$$

with (real) wavenumber k and (complex) frequency ω. The latter can be directly written in terms of the growth rate and the period used in section 2. In fact, this is the formulation that has actually been used in this work.

Due to the notion of zonal Fourier decomposition for single wavenumbers, a natural limitation of the two methods used in this study is as follows. Since the wavelength for a specific zonal wavenumber is shorter in higher latitudes than in lower ones, the zonal scale of POP patterns or unstable modes must decrease with increasing distance from the equator. Moreover, the Fourier coefficients describe global patterns around whole latitude circles. Thus, it is not possible to identify regional patterns or patterns with features of equal scale in well-separated latitude bands as, for example, the Pacific–North America (PNA) pattern.

4. Results

The results of the above-described POP analyses and linear stability analyses are given first for the Northern Hemisphere (section 4a). After presenting a general overview for all wavenumbers, attention is drawn to wavenumber 8, as an example. The structure of the patterns is given in detail for this case. The Southern Hemisphere is treated in subsection 4b. A listing of all POPs that were found to be significant and corresponding unstable eigenmodes is given in the Appendix for reference.

a. Northern Hemisphere

In Fig. 2, three characteristic numbers resulting from a POP analysis are shown for the wavenumber k = 5–9 analyses of the Northern Hemisphere geopotential height fields. The bars in Fig. 2a denote the explained variances for the POPs that are found to be most significant. For each POP **P**, this quantity is the percentage of wavenumber k variance that is accounted for by **P**, together with its coefficient time series $z(t)$, averaged over space. In almost all cases a POP will be considered significant if it explains at least 5% of the total variability that is caused by waves of the respective wavenumber (see also Appendix). Since, in this study,

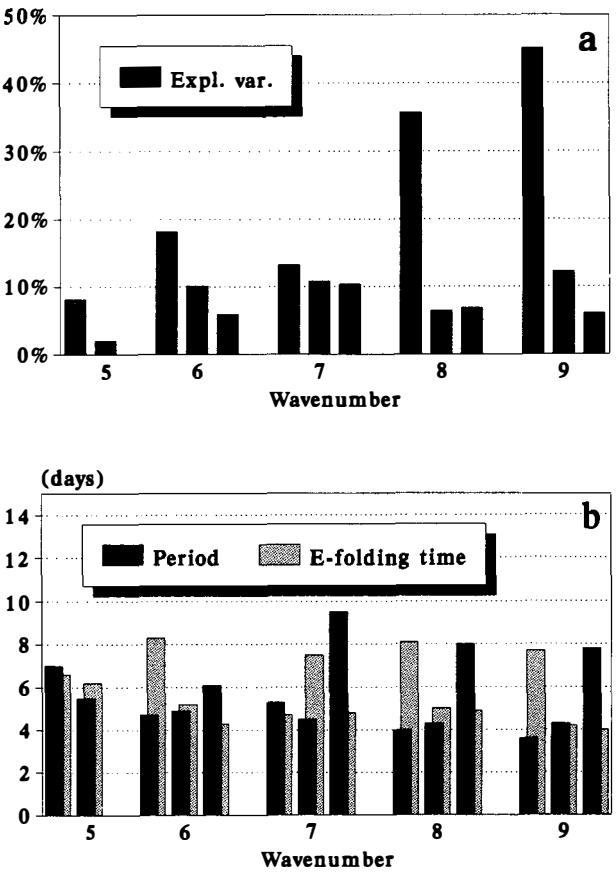

FIG. 2. POP analyses of twice-daily geopotential height in the Northern Hemisphere for the three winters DJF 1984/85–1986/87 and for zonal wavenumbers 5–9. Shown are the (a) explained variances and (b) the periods and e-folding times of the respective POPs. The numbering of the POPs in the text refers to the ordering with respect to decreasing explained variances for each wavenumber.

each POP analysis only uses the data of the particular wavenumber under consideration, this number is only a measure of the significance of the POPs in each single analysis. It does not say anything about the relative importance of POPs for different wavenumbers. Also note that unlike the explained variances of EOFs, these quantities are not additive because POPs are not necessarily (statistically) orthogonal. The ordering of the POPs for each wavenumber will be used throughout the paper and refers to the explained variance as a measure of significance. In Fig. 2b the POPs are grouped together for each wavenumber, displaying the oscillation period (dark shaded bars) and the *e*-folding time (light shaded bars).

It can be seen that the explained variances range from about 10% to 45%, the signals getting clearer with increasing wavenumber. On the whole, the periods lie between 4 and 8 days. For some of the POPs, the *e*-folding time is two times a period, which means that the patterns can perform two oscillation cycles (4) before being damped with a factor of $1/e$. For the other POPs, the oscillations can be seen for at least half of a period before they are *e*-folded.

The periods of the POPs are in good accordance with the findings of other studies. In the Introduction, the space–time power spectrum of a five-winter geopotential height field in the Northern Hemisphere was shown. If the POP periods are inserted into this plot (Fig. 1), it can be seen that the POPs reflect the variability of the atmospheric circulation in this wavenumber range. The picture at least shows fairly good agreement with the relationship between the space and time scale found in Fraedrich and Böttger's study. The variances of the coefficient time series associated with the POPs (not shown) indicate how the power is distributed over the different wavenumbers. They are also in agreement with the position of the power maxima at wavenumbers 5 and 6 in Fig. 1.

It should be stressed that the explained variance is only to be understood as a measure of significance in a nonstatistical sense. Since a POP analysis is multivariate, there is no formalism at hand to state, in a probabilistically strict sense, a hypothesis about the POP patterns that could be tested for significance. If the time series is long enough we could instead derive the POPs for disjoint independent subsets. If each of these analyses yields POPs with similar characteristics and spatial structures, then the corresponding POP of the original analysis may be assumed to describe some "real" phenomenon that is worth interpreting. As an example, a POP analysis has been carried out separately for each of the three winters, in the case for wavenumber 8 and in the Northern Hemisphere. The results were indeed fairly similar to those discussed in this paper.

Figure 3 summarizes the normal modes of the linear stability analysis. The growth rate of the most unstable modes (Fig. 3a, left bar in each group) increases from its smallest value at wavenumber 5 to a maximum of 0.45 for wavenumber 8, which means that the amplitude of an initial wavenumber 8 disturbance has grown by a factor of *e* after about 2 days. The growth is almost constant for wavenumbers 7–9. The periods of these modes (Fig. 3b, left bars) have values between 3.5 and 6.5 days, with decreasing periods for smaller wavelengths. The characteristic numbers for the second-most and the third-most unstable normal modes are also shown in the diagram.

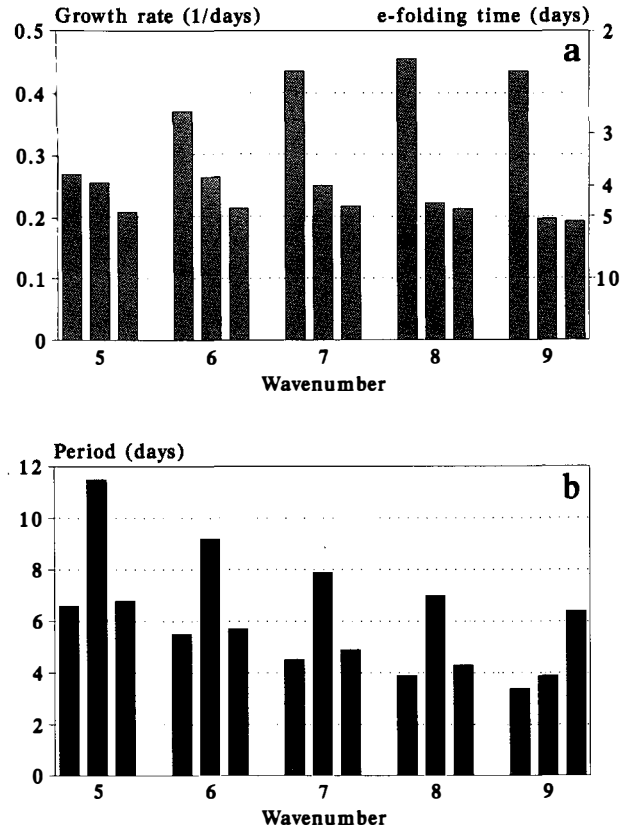

FIG. 3. Linear stability analyses for zonal wavenumbers 5–9 of the discretized quasigeostrophic vorticity equation linearized about a climatological zonally symmetric basic state from three winter (DJF 1984/85–1986/87) wind fields in the Northern Hemisphere. Shown are (a) the growth rates and (b) periods of the three most unstable waves. The right axis in (a) expresses the growth rate in terms of *e*-folding time.

Note that the predominant waves predicted by linear instability theory on the basis of growth rate are wavenumbers 7–9, whereas the wave power maxima in the atmosphere occurs at wavenumbers 5 and 6 (Fig. 1). In two papers, Gall (1976a,b) suggests several nonlinear processes that are absent in the stability analysis and may be responsible for this discrepancy in zonal-scale selection. Interaction between a growing wave and the zonal flow leads to a decrease of the vertical shear of the zonal wind and an increase of the zonal-mean static stability, especially in the lower troposphere. Therefore,

the most rapid decrease of growth occurs at lower levels and, consequently, the long waves can reach greater amplitudes than short waves do. Another reason may be wave–wave interactions that lead to an energy cascade from small scales to larger scales. Also, surface friction is more effective in slowing down the growth of short waves than long waves.

The purpose of this paper is, besides describing the application of the POP analysis to tropospheric waves itself, to compare an empirical and a theoretical approach to the determination of the normal modes of the atmosphere. This has already been mentioned in the Introduction. A first indication that this may be a promising task is given by the comparison of the periods of POPs and unstable waves. Figure 4 jointly displays for each wavenumber the periods of the three most unstable waves from the stability analysis and the three most significant POPs. It can be seen that in quite a few cases the periods of an unstable mode and a POP are located very close to each other so that both analyses possibly yield the same waves.

This must, of course, be verified by investigating the spatial structure of the modes, and by other diagnostics. As an example, most of the further treatment will be given in detail for wavenumber 8. Information on the other wavenumbers will be provided where appropriate.

Figure 5 shows the phase (upper row) and amplitude (lower row) structure of POP 1 in four latitude–height diagrams. This POP explains 35% of the total wavenumber 8 variance. In the whole region, the amplitudes of the real (left column) and imaginary (right column) part are almost equal, with maximum values in the upper troposphere and at 45°N. A small secondary maximum is indicated at the bottom. In the region of significant amplitudes, the phases of both parts have a very similar distribution and are shifted by about 90°, with the imaginary part being west of the real part. Together with the POP cycle (4), this gives the picture of a pattern propagating in the eastward direction. In order for this conception to be valid, it is also required that the real and imaginary parts of the corresponding complex coefficient time series be out of phase by a quarter of a period. This has been verified by computing the cross spectrum of both parts (not shown), yielding maximum power and a phase shift of 90° at the POP period of 4 days. The coherence is above the 99% confidence limit.

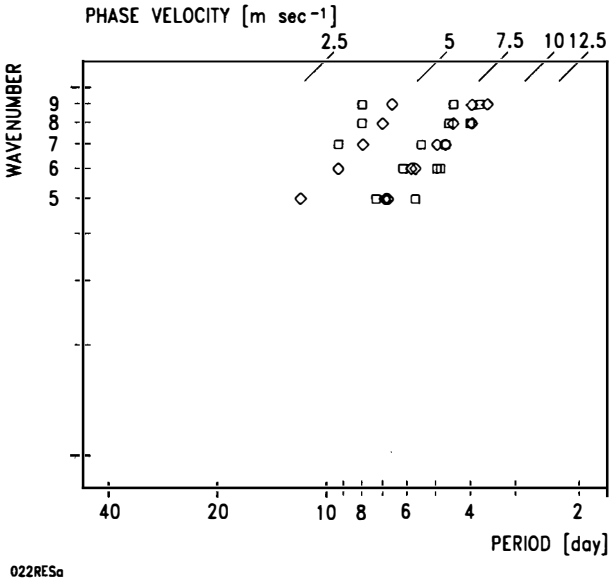

FIG. 4. Periods of the first three POPs (squares; only two for wavenumber 5) and the three most unstable normal modes (diamonds) from the Northern Hemisphere analyses plotted against zonal wavenumbers 5–9.

The phases in Fig. 5 tilt westward, with a phase difference of about 50° (corresponding to 50/8° longitude) between the surface and 300 hPa. Above 300 hPa, the phase is nearly constant. There is only a small dependence of the phase with latitude, indicating no meridional momentum transport; the lines of constant phase are only slightly curved at upper levels. This horizontal structure and its eastward propagation is more visible in cross sections of the Fourier-reconstructed wave in the 200-hPa level (Fig. 6).

The most unstable mode resulting from the linear stability analysis for wavenumber 8 is plotted in Fig. 7. As has already been mentioned in section 3, only one pattern needs to be shown since the analysis is restricted to longitudinally independent features. The vertical phase gradient in midlatitudes and the position of the amplitude maximum in the upper troposphere are in good coincidence with POP 1. A striking difference is the large-amplitude maximum of the unstable mode at the bottom. Similar structures were found in unstable modes found by Valdes and Hoskins (1988). However, when they included frictional effects at the bottom in their linearized primitive equation model by means of Ekman pumping, this lower maximum disappeared. So it can be assumed that bottom friction would also bring the vertical profile of the unstable mode in our calculation closer to that of the POP. Also, nonlinear effects that influence the POP via the observation data may be suitable to explain this difference. Simmons and Hoskins (1976) showed unstable primitive equation modes that were very similar in structure to the above modes. In particular, the slight meridional phase curvature seen in the POP matched very well.

Thus, it can be stated that both the most significant POP and the fastest growing normal mode describe the same atmospheric oscillation, and the POP can be attributed to the genesis of baroclinic waves due to the instability of the basic flow.

POPs with structures similar to the wavenumber 8 POP that was just described are found for almost all wavenumbers. We have also found some POPs with a typical amplitude–phase structure that are only con-

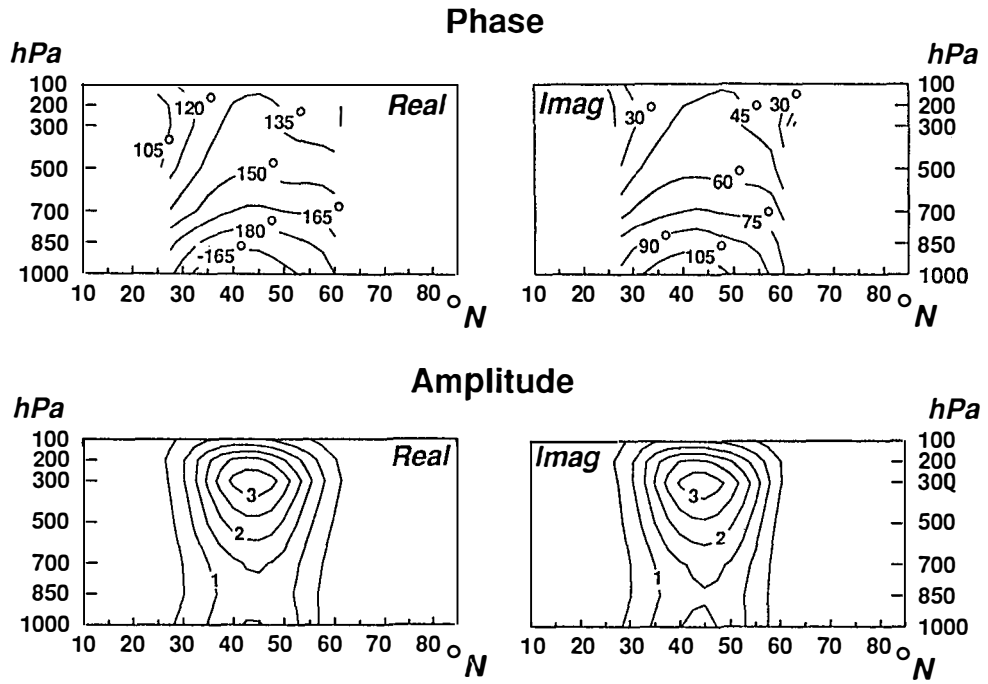

FIG. 5. The most significant POP of a POP analysis of twice-daily geopotential height in the Northern Hemisphere for the three winters (DJF) 1984/85–1986/87 and for zonal wavenumber 8. The oscillation period is 4 days, and the *e*-folding time is 8.6 days. The real part $\mathbf{P}^1$ (left) and imaginary part $\mathbf{P}^2$ (right) of the POP $\mathbf{P}$ are represented by phase patterns Ξ^1 and Ξ^2 (top) and amplitude patterns $\mathbf{A}^1$ and $\mathbf{A}^2$ (bottom). The evolution of the pattern is defined by the sequence . . . → imag → real → −imag → −real → imag → . . . . The absolute values of the amplitude patterns are arbitrary. The phase is only plotted where the amplitude is at least 12% of it's maximum value.

fined to selected wavenumbers. For waves 6 and 9, POPs are found with a phase tilt in the southeast–northwest direction, especially at lower levels. Their region of maximum amplitudes at upper levels is divided into a primary and a smaller secondary maximum. The 500-hPa cross section of POP 3 for wavenumber 6 (Fig. 8) clearly shows this horizontal phase and amplitude relationship with a strong meridional

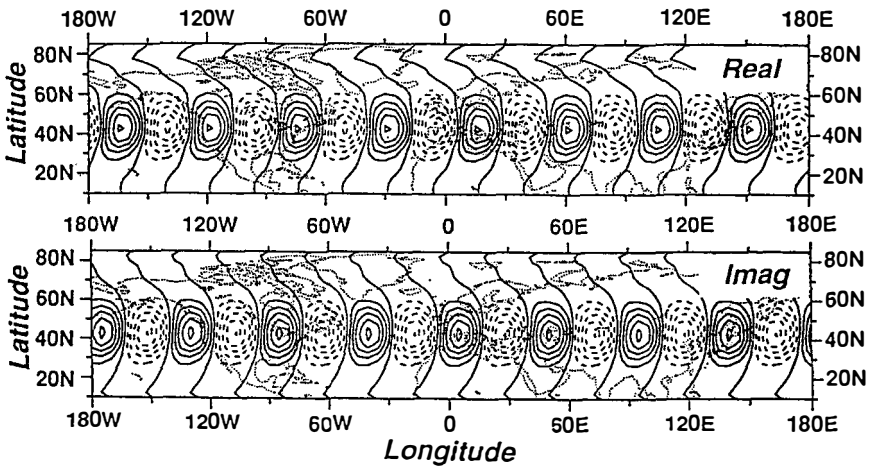

FIG. 6. Cross section at the 200-hPa level of the POP, which is shown in Fig. 5. The values of amplitude and phase at each latitude have been Fourier reconstructed to show the horizontal wave patterns of real (top) and imaginary (bottom) parts. The evolution of the pattern is defined by the sequence . . . → imag → real → −imag → −real → imag → . . . . The absolute values of the contour lines are again arbitrary.

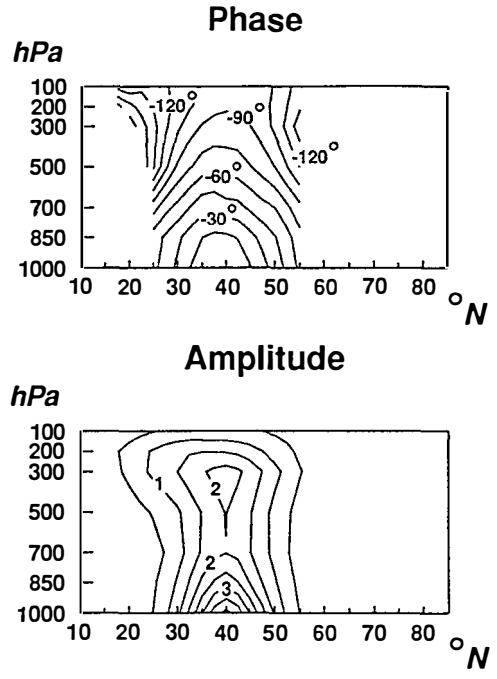

FIG. 7. The most unstable zonal wavenumber 8 mode on the Northern Hemisphere identified in the stability analysis of the discretized quasigeostrophic vorticity equation linearized about an observed zonal mean state in northern winter. The growth rate is 2.2 days (that is, an initial amplitude is amplified by a factor of e in 2.2 days), and the oscillation period is 3.9 days. Since the unstable mode $\mathbf{Q}$ is completely determined by the real part, only the amplitude and phase patterns $\mathbf{A}^1$ and Ξ^1 of $\mathbf{Q}^1$ have to be shown. Component $\mathbf{Q}^2$ is then given by $\mathbf{A}^1$ and $\Xi^1 - \pi/2$. The patterns have been vertically interpolated to the pressure grid used in the POP analyses.

momentum transport. But there is also a mode from the linear stability analysis corresponding to this POP with respect to phase velocity and three-dimensional structure (Fig. 9). Thus, the POP analysis is also able to identify unstable modes that play a totally different role in the process of instability. A similar relationship can be established for POP 1, and the third most unstable mode for $k = 7$, as well as POP 2 and the second most unstable mode for $k = 9$, which are characterized by a distinct dipole structure in lower levels.

In addition to the above-described modes, the POP analyses also yield patterns that explain some variance, which are not found in the linear stability analysis. POP 3 for wavenumber 8 is an example (Fig. 10). It has a period of 4.3 days and a decay time of 5 days with an explained variance of 6.4%. The amplitude distributions of the real and imaginary parts are again very similar, with a broad maximum in the upper troposphere and greatest values at 35°N. The patterns are 90° out of phase. In the vertical, the wave has only a slight westward tilt, but there is a strong meridional phase gradient resulting in a southwest–northeast-tilted wave. This POP is reminiscent of the latitudinal structure of baroclinic waves in their nonlinear decay phase, which were identified by Hoskins and Simmons (1978) with a primitive equation model. They are characterized by a strong northward transport of momentum that corresponds to a distinct Rossby wave dispersion. POP 3, $k = 7$, and POP 2, $k = 8$ have a similar amplitude structure but, besides having only small vertical phase tilt, phases are also almost constant with latitude where amplitudes are significant. This nearly constant phase in the meridional plane means that there is no meridional transport of both momentum and heat. These patterns could characterize the end phase in the life cycle of baroclinic waves.

As a result of these findings, section 5 has as its subject the interpretation of the POPs in terms of the life cycle of baroclinic waves. But before proceeding to this point, the Southern Hemisphere is treated first.

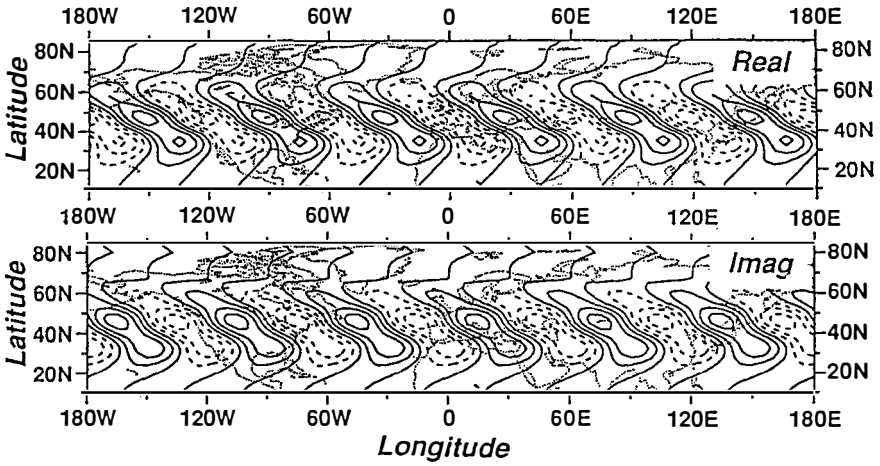

FIG. 8. As in Fig. 6 but for the 500-hPa cross section of the wavenumber 6 POP that explains the third-most of the wavenumber 6 variance. The oscillation period is 6.1 days, and the e-folding time is 4.3 days.

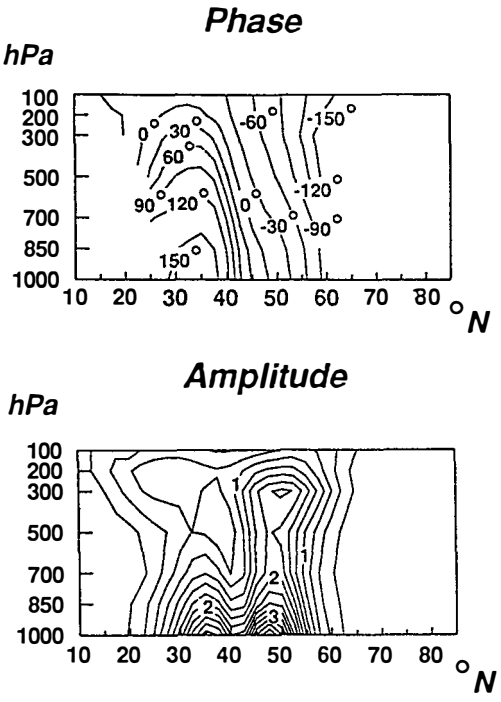

FIG. 9. As in Fig. 7 but for the third-most unstable mode of the wavenumber 6 stability analysis. The growth rate is 4.7 days, and the oscillation period is 5.7 days.

b. Southern Hemisphere

The results for the DJF Southern Hemisphere are summarized here and are described to the extent to which they differ from what has been shown so far.

Figure 11 displays the characteristic numbers for the POP analyses and should be compared to Fig. 2. The first thing that can be noticed is that there are more POPs that are found to be significant than in the Northern Hemisphere. Their explained variances are generally higher, although the peak value of 45% for wavenumber 9 in the NH is not reached. Also, the damping times are considerably larger in the Southern Hemisphere, indicating that the waves are retaining their amplitude longer than NH waves do. These facts may be an indication for the well-known observation that transient features in the Southern Hemisphere tend to be longitudinally more global than in the NH. In the NH they are often confined to local storm-track areas. This behavior, in turn, matches the analysis techniques in this study, namely, the assumption of zonal symmetry and the restriction of the analyses to zonal wavenumber space. As a consequence, the signals are easier to detect for the POP analysis and fit better to the POP model in the SH than in NH. The periods of the POPs are very similar to that of the NH POPs and fall again into the band between 4 and 7 days. The variances of the coefficient time series of the POPs indicate maximum power at wavenumbers 6 and 7, whereas the contribution of wavenumbers 8 and 9 is fairly small.

Figure 12 shows the periods and growth rates of the three most unstable waves of the SH linear stability analysis. Most periods are again around four days. Compared to Fig. 3, the growth curve for the most unstable modes has a more distinct maximum at wavenumber 8, and the modes generally grow more

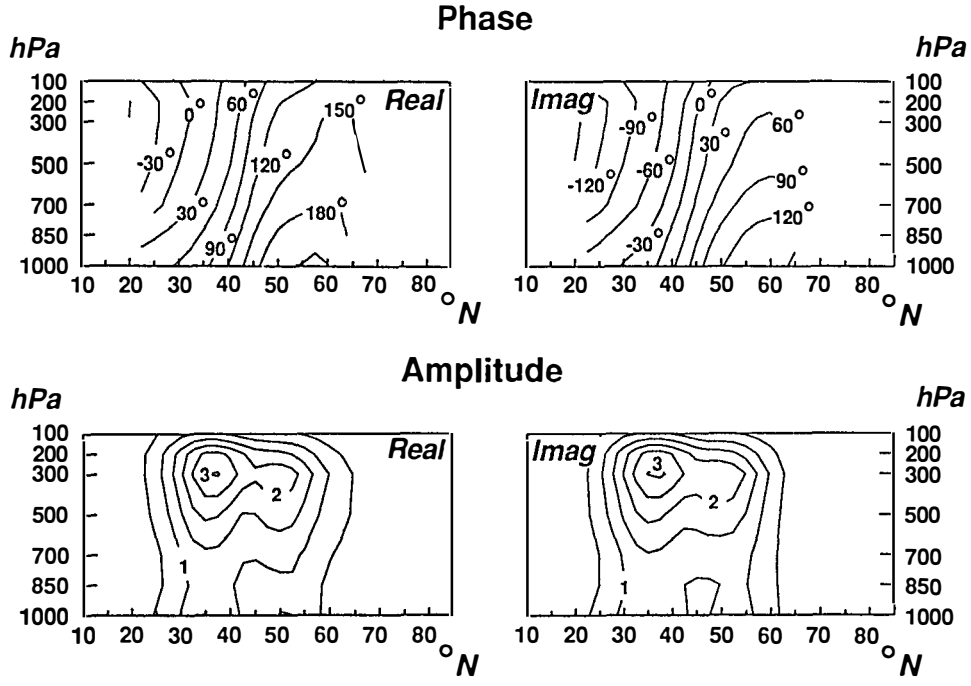

FIG. 10. As in Fig. 5 but for the wavenumber 8 POP that explains the third-most of the wavenumber 8 variance. The oscillation period is 4.4 days, and the *e*-folding time is 5 days.

slowly than in the Northern Hemisphere. This reduced instability is related to the differences in the strength and structure of the NH and SH mean zonal winds used in the stability analysis. The comparison between the greater *e*-folding times and the smaller growth rates in the SH analyses shows that POP *e*-folding times are not necessarily a measure of how unstable a flow is. We will come back to this point in the discussion section (section 6).

The comparison of POP periods with the periods for the most unstable modes again indicates a good correspondence between the two methods. Though not shown, this correspondence has been confirmed by considering diagrams of spatial structure in the same manner as described above (see also section 5). Only for wavenumber 9 does the stability analysis yield no modes that can be identified with POPs. But for this wavenumber the growth rates are generally very small, so that waves of this scale are not preferred by the instability process in the theoretical model. In the SH the POP analyses identify modes with northwest–southeast phase tilt (instead of southwest–northeast in the NH) that can be attributed to the decay phase of baroclinic waves. This tilt corresponds to a poleward momentum flux in the Southern Hemisphere. Modes

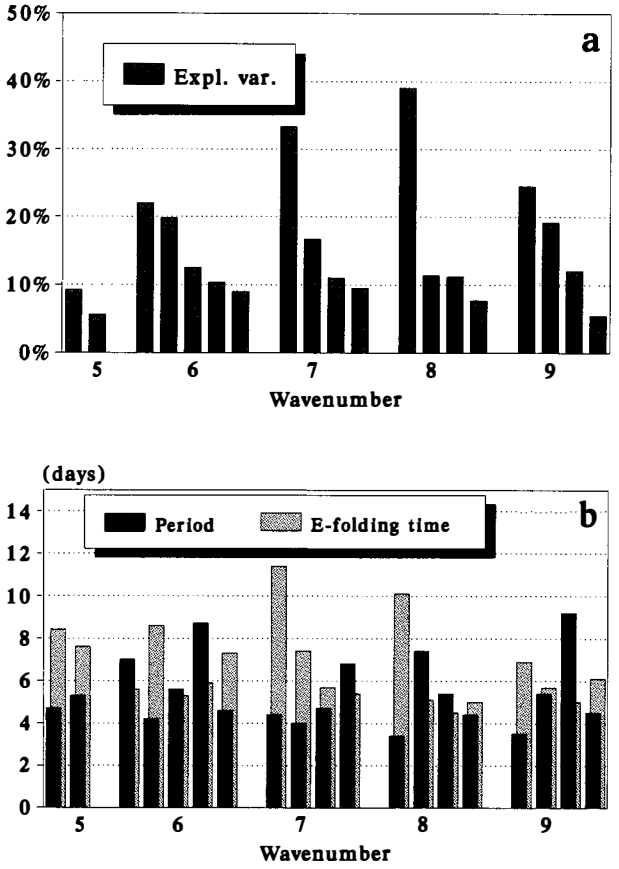

FIG. 11. As in Fig. 2 but for the POP analyses in the Southern Hemisphere.

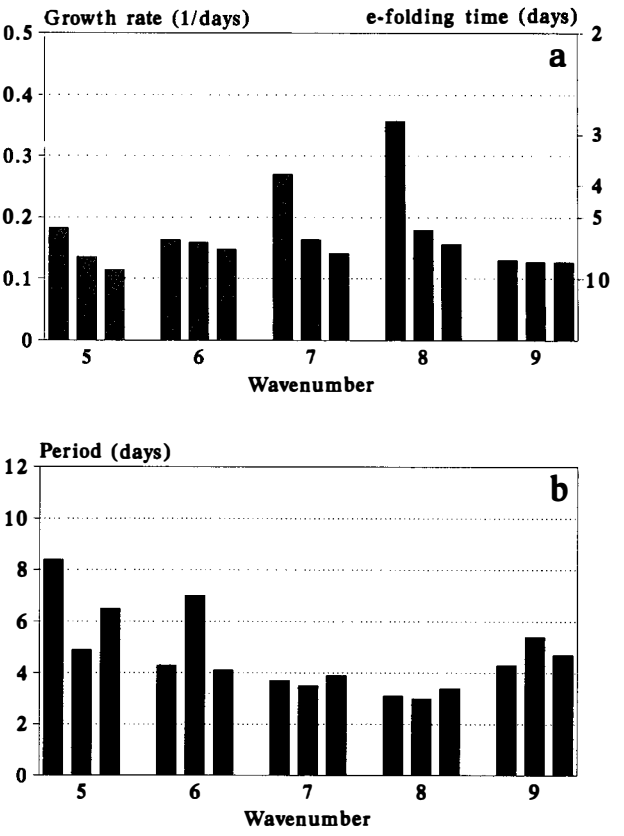

FIG. 12. As in Fig. 3 but for the stability analyses in the Southern Hemisphere.

with an equatorward momentum flux, that is, southwest–northeast phase tilt, which were found in the Northern Hemisphere, are not present in the Southern Hemisphere, either in the stability analysis or in the POP analysis.

5. Life cycle of baroclinic waves

A valuable tool for investigating disturbances on top of a zonal mean flow are Eliassen–Palm (EP) cross sections that jointly display the Eliassen–Palm flux vector and its divergence in latitude–height diagrams.

The Eliassen–Palm flux is a vector

$$\mathbf{F} = \mathbf{F}(\theta, z) = (\mathbf{F}_\theta, \mathbf{F}_z)$$

in the meridional plane (θ, z), where $\mathbf{F}_\theta$ is the negative of the northward flux of eastward momentum, and $\mathbf{F}_z$ is the northward flux of heat. Since each POP pattern corresponds to geopotential height, it is straightforward to compute the EP fluxes of the POPs in a quasigeostrophic framework (Grieger and Schmitz 1984).

Plots of the arrows defined by $\mathbf{F}$ show the wave energy propagation from one latitude and height to another and the relative magnitudes of meridional heat and momentum fluxes. Contours of the EP flux divergence $\nabla \cdot \mathbf{F}$ describe the meridional flux of potential vorticity and the net propagation of wave activity. They

also represent the wave–zonal flow interaction. Negative divergence, that is, convergence, of the EP flux means that the zonal flow is decelerating and feeding energy into the disturbance (neglecting the contribution of a residual meridional circulation). A detailed review of the dynamical information contained in EP diagrams is given by Edmon et al. (1980).

Following Randel and Stanford (1985b), the evolution of baroclinic waves during their life cycle is connected with typical changes in the EP cross section. A strong meridional gradient of zonal-mean temperature at low levels allows for the transfer of energy from the basic flow into a growing wave. In terms of the EP flux vectors, this shows up as large arrows in the lower troposphere, which are directed upwards. During the linear growing phase, this poleward heat flux is connected with a vertical propagation of wave activity from the surface into the middle troposphere and results in a convergence of the EP flux vectors in the mid-to-upper troposphere.

At wave maturity, the heat flux is distributed over the whole troposphere, resulting in a smaller growth rate and convergence in the upper region. Following this stage, the heat flux lessens at the lower levels and the direction of wave activity propagation turns equatorwards in the upper troposphere. This quasi-horizontal wave propagation from midlatitudes toward the subtropics is accompanied by strong, poleward, momentum fluxes at upper levels. The wave is in its phase of barotropic decay. This stage is associated with an extension of the region of divergent EP flux to the lower-to-middle troposphere and an upper region of strong convergence that is located more equatorward than initially.

The results of the POP analyses and the linear stability analyses can now be interpreted in terms of the above-described life cycle of baroclinic unstable waves

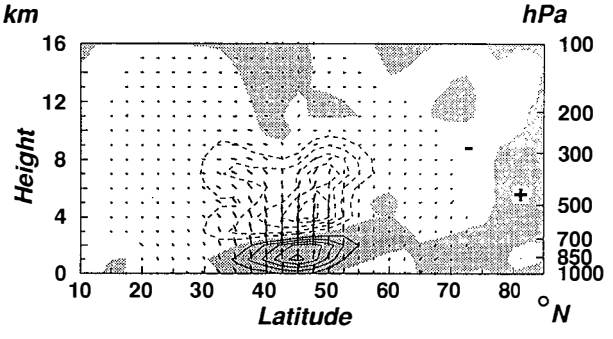

FIG. 13. Eliassen–Palm diagram for the real part of the POP, which is shown in Fig. 5. The vertical coordinate is geometric height as used in the linear stability analysis, and the pressure levels used in the POP analysis are inserted at the right axis. Regions of positive divergence are shaded. The Eliassen–Palm flux (arrows) is in units of ($m^3 s^{-2}$, $m^3 s^{-2}$), and it's divergence (contours) is in units of ($m^2 s^{-2}$). The vertical component of the arrows has been scaled by a factor of 100. The length of the arrows and the absolute values of the flux divergence are arbitrary since the amplitude of the POP pattern is arbitrary.

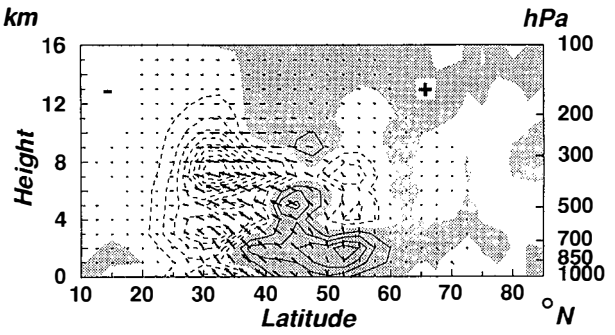

FIG. 14. As in Fig. 13 but for the POP shown in Fig. 10.

by means of EP cross sections. As an example we focus again on the wavenumber 8 of the Northern Hemisphere analyses.

The EP diagram for POP 1 of the wavenumber 8 analysis (Fig. 13) shows the features of the linear growing phase well and, thus, confirms the previously given interpretation of this POP. The lack of meridional momentum transport, as indicated by the weak, first component $\mathbf{F}_\theta$ of the EP flux vector, has already been noted in section 4a (Fig. 6). The upward-directed arrows at the lower levels show that northward heat flux $\mathbf{F}_z$ and the vertically propagating wave activity are the primary mechanisms connected with this mode. There is an EP flux divergence at lowest levels and a convergence at mid-to-upper levels in midlatitudes. This is consistent with a baroclinic energy conversion from the basic flow to the disturbance that is, thus, growing.

Note that it is only necessary to consider the EP diagram of, say, the real part of a POP because both parts are very similar, except for a zonal shift and the fact that only zonally averaged quantities enter the EP flux.

Not unexpectedly, the EP diagram for the most unstable mode of the stability analysis for wavenumber 8 (not shown) is similar to Fig. 13.

The EP diagram of POP 3 for wavenumber 8 is presented in Fig. 14. The dominating feature is the distinct equatorward tilt of the arrows, especially in the upper troposphere. Thus, there is a strong equatorward wave-activity flux at upper levels. Poleward momentum fluxes are important for this mode and have already showed up in the spatial structure of this POP as a horizontal southwest–northeast tilt (Fig. 10). The region of strong EP flux convergence is concentrated in the mid-to-upper troposphere and has shifted equatorward, compared to POP 1.

These features are all in very good qualitative agreement with the characteristic behavior of unstable waves in their decay phase, as observed by Randel and Stanford (1985a,b). Thus, the structure of the EP cross section substantiates the conjecture made at the end of section 4a and identifies POP 3 with the barotropic decay phase of a baroclinically unstable wave.

For almost all wavenumbers of the NH and SH POP analyses, similar relationships can be established (see

Appendix). The POP analysis is, thus, able to extract patterns that can be attributed to different phases in the life cycle of baroclinic unstable waves.

6. Summary and discussion

In this paper, medium-scale traveling waves in the atmosphere have been considered normal modes of a linear dynamical system. The system has been formulated in a semispectral representation, and only waves of zonal wavenumbers 5–9 have been considered. The system matrix of this linear system has been obtained in two conceptually different ways. In one case, it was estimated from observation data of three winter (summer, respectively) seasons (POP analysis) and in the other case it was derived theoretically from the quasigeostrophic equations, making assumptions on the smallness of the disturbances (linear stability analysis).

The most unstable waves resulting from the stability analysis can be found in the POP analysis, too. Also, some modes with smaller growth rates have corresponding POPs. The respective waves coincide very well with respect to the oscillation period and three-dimensional structure. Thus, these POPs can be interpreted as baroclinic waves in their linear growing phase. The results show a very nice equivalence between the two approaches used, namely, the empirical method that uses atmospheric observations and the theoretical method that uses first-order dynamical reasoning. Since the POPs result from an observational analysis, in a way this coincidence also shows the appropriateness of the severe simplifications used in the conventional stability analysis in order to investigate waves in the atmosphere.

At this point a slight inconsistency between the two analysis techniques should be mentioned that refers to damping times and growth rates. Under the assumption of a stationary data time series, a POP analysis always gets damped POPs with corresponding eigenvalues $|\sigma| < 1$ because any eigenvalue with $|\sigma| > 1$ would characterize an exploding solution of (3). By estimating the matrix $\mathbf{A}$ of the linear system (1) from the data, the POP analysis of a particular zonal wavenumber preferentially "sees" an oscillation when it is fully developed, with noise relatively small, and when damping occurs because of nonlinear and other processes. In the stability analysis the system matrix $\mathbf{A}$ is derived from a linearization of a nonlinear dynamical equation, where a small perturbation is superimposed on a basic state. This system contains the potential of amplifying solutions and, actually, these are the solutions we are interested in. In this case, eigenvalues with $|\sigma| \geq 1$ describe the formation and growing of oscillations, which the POP analysis eventually detects.

The POP analysis also reveals waves that are not found in the linear stability analysis. Their spatial structure and wave energetics are reminiscent of the nonlinear decay phase of baroclinic waves. Using the notion of the instability of a basic flow, this stage can only be described by integrating more complex (nonlinear) models in time. However, as Simmons and Hoskins (1978) have shown, nonlinearity is mainly important from the point where the linear growth of a wave comes to an end and the barotropic decay begins. The evolution of the wave in an upper level, following this transition point, can be approximated fairly well by quasi-horizontal Rossby wave propagation mechanisms. This may be a reason that the linear method of POP analysis can also describe this phase, although nonlinear mechanisms play a role.

Thus, the POP analysis has proven to be an easy-to-use method to extract zonally propagating midlatitude waves from observational data. However, the limitation to zonal wavenumber space that has been made restricts the method to representing only regularly developing waves of a longitudinally global nature. Although the results are reasonable, this is not really the behavior of the atmosphere. Especially in the Northern Hemisphere, the variability is confined to local storm track areas, which means that waves have large amplitudes only in certain bands of longitude. In view of this, the patterns presented in this study for the Northern Hemisphere have to be understood as being valid only in certain regions and as being damped out after a time of propagation.

In order to better account for the facts we have described, it would be necessary to consider wave packets in the POP analysis instead of single zonal wavenumbers or to do the analysis in spherical harmonics space. This would also yield information about the degree to which the different wavenumbers are responsible for the total variability.

It can also be expected that the above extensions would be able to better represent the growth and decay of baroclinic waves. Since the waves have big amplitudes in preferred regions, the growth will occur at certain longitudes and the decay will happen at others. For each stage, the corresponding complex POP pattern could have, for example, an imaginary part with its maximum amplitudes in the region of the genesis of the wave and a real part with greater amplitudes east of this. Since the real part describes the wave a quarter of a period after the imaginary component is valid, this would describe the actual growth of the wave and would, thus, solve the above-mentioned inconsistency between POP analysis and stability analysis.

Eventually, by looking at the coefficient time series of these POPs, it should be possible to describe certain cases of the life cycle of baroclinic waves in observational fields or model results. We have made a preliminary attempt in this direction by starting from the trivial fact that the decay of a wave takes place a certain time after its growth, but no clear correlation (lagged) has been established between the coefficient time series of the "growing phase" and the "decay phase" POPs.

Acknowledgments. The authors would like to thank Grant Branstator for useful discussions and his very valuable comments on the manuscript. The Appendix

is specially dedicated to Ernst Maier-Reimer. He attended the first lecture given by the first author and prevented him from presenting any more tables in lectures after that. Hopefully, he will not disapprove of the form chosen herein in a written paper.

The data used in this study were taken from the ECMWF–WMO global analysis datasets 1980–87 of the European Centre in Reading, England, with the permission of the Deutscher Wetterdienst (DWD), Germany.

APPENDIX

Results of Section 4

Tables A1 and A2 list all significant POPs in terms of their characteristic numbers—*e*-folding time, oscillation period, and explained variance—for the Northern and Southern hemispheres, respectively. In this paper, significance of a POP has always been measured in terms of the explained variance as well as the ordering within each wavenumber that refers to this number. It should be noted, however, that this number is not the only criterion upon which useful POPs are chosen from the totality of modes of a POP analysis. Additional information that aids the assessment of the results can, for example, be obtained by looking at the *e*-folding times, the coefficient time series (cross-spectral analysis), and plots of the patterns.

A class name is assigned to each POP in the tables according to the different three-dimensional structures described in section 4. Most important is class A, which describes the modes being attributed to the linear growing phase of unstable baroclinic waves, and class B, which corresponds to the decay phase. The classes are characterized by the following structure of the patterns:

Class A—one amplitude maximum in midlatitudes and the upper troposphere; vertical westward phase tilt from the bottom to 500–300 hPa in the region of significant amplitudes, nearly constant phase above that level; little dependence of phase with latitude, lines of constant phase are only slightly curved.

Class B—a broad amplitude maximum in the upper levels sometimes showing up as a double maximum; westward phase tilt with height; strong meridional phase tilt in southwest–northeast (Northern Hemisphere) or northwest–southeast (Southern Hemisphere) direction, especially at upper levels.

Class C—amplitudes as in B; almost constant phase in the region of large amplitudes;

Class D—double amplitude maximum; meridional phase tilt in northwest–southeast (Northern Hemisphere) or southwest–northeast (Southern Hemisphere) direction, especially at lower levels.

Class E—distinct dipole structure of both amplitude and phase distribution, especially at lower levels.

Small departures from these structures might, of course, happen. In classifying the patterns, reference has also been made to the Eliassen–Palm cross sections that are typically connected with the different struc-

TABLE A1. *POP*s and unstable normal modes in the Northern Hemisphere for zonal wavenumbers 5–9. The number (No.) of a *POP* refers to its position among all *POP*s of an analysis for a particular wavenumber in terms of decreasing explained variance. The same is true for the unstable modes but with respect to decreasing growth rate. The "growth" of an unstable mode (second column from the right) is the inverse of the growth rate, that is the time after which an initial disturbance has grown by a factor of *e*. *POP*s and unstable modes that are printed on one line have a similar period and a structure that is described by the classes A–E. The *e*-folding times, growth, and periods are given in days, explained by variance in percent.

	POP analysis					Unstable waves		
Wavenumber	No.	*e*-folding time	Period	Explained variance	Class	No.	Growth	Period
5	1	6.6	7.2	8.1	B	—	—	—
	2	6.2	5.5	2.0	A	1	3.7	6.6
6	1	8.3	4.7	18.3	B	—	—	—
	2	5.2	4.9	10.1	A	1	2.7	5.5
	3	4.3	6.1	5.9	D	3	4.7	5.7
7	—	—	—	—	A	1	2.3	4.5
	1	4.7	5.3	13.2	E	3	4.6	4.9
	2	7.5	4.5	10.8	B	—	—	—
	3	4.8	9.5	10.3	C	—	—	—
8	1	8.1	4.0	34.7	A	1	2.2	3.9
	2	4.9	8.0	6.8	C	—	—	—
	3	5.0	4.4	6.4	B	—	—	—
	—	—	—	—	E	3	4.7	4.3
9	1	7.8	3.6	45.1	A	1	2.3	3.4
	2	4.2	4.3	12.2	E–D	2	5.1	3.9
	3	4.0	8.0	6.0	B	—	—	—

TABLE A2. As in Table 1 but for the Southern Hemisphere.

	POP analysis					Unstable waves		
Wavenumber	No.	*e*-folding time	Period	Explained variance	Class	No.	Growth	Period
5	1	8.4	4.7	9.2	A	2	7.4	4.9
	2	7.6	5.3	5.6	E	—	—	—
6	1	7.0	5.6	22.0	A	2	6.3	7.0
	2	8.6	4.2	19.8	A	1	6.1	4.3
	3	5.3	5.6	12.5	C	—	—	—
	4	5.9	8.7	10.3	B	—	—	—
	5	7.3	4.6	9.0	A	—	—	—
7	1	11.4	3.4	33.3	A	1	3.7	3.7
	2	7.4	4.0	16.7	B	—	—	—
	3	5.7	4.7	11.0	C	—	—	—
	4	5.4	6.8	9.5	B	—	—	—
8	1	10.1	3.4	39.1	A	1	2.8	3.1
	2	5.1	7.4	11.4	B	—	—	—
	3	4.5	5.4	11.2	B	—	—	—
	4	5.0	4.4	7.7	E	—	—	—
9	1	6.9	3.5	24.6	A	—	—	—
	2	5.7	5.4	19.2	A	—	—	—
	3	5.0	9.2	12.1	B	—	—	—

tures. The rightmost columns of Tables A1 and A2 list the most unstable modes from the linear stability analyses that approximately fall in one of the above classes. They are numbered in terms of their growth rates. POPs and unstable modes that describe the same feature are printed on one line. This correspondence has been evaluated from the periods, the three-dimensional structures, and the Eliassen–Palm cross sections.

REFERENCES

Blackmon, M. L., Y. H. Lee, and J. M. Wallace, 1984a: Horizontal structure of 500 mb height fluctuations with long, intermediate, and short time scales. *J. Atmos. Sci.*, **41,** 961–979.

——, ——, and H.-H. Hsu, 1984b: Time variation of 500 mb height fluctuations with long, intermediate, and short time scales as deduced from lag-correlation statistics. *J. Atmos. Sci.*, **41,** 981–991.

Charney, J. G., 1947: The dynamics of long waves in a baroclinic westerly current. *J. Meteor.*, **4,** 135–162.

——, and M. E. Stern, 1962: On the stability of internal baroclinic jets in a rotating atmosphere. *J. Atmos. Sci.*, **19,** 159–172.

Eady, E. T., 1949: Long waves and cyclone waves. *Tellus,* **1,** 33–52.

Edmon, H. J., B. J. Hoskins, and M. E. McIntyre, 1980: Eliassen–Palm cross sections for the troposphere. *J. Atmos. Sci.*, **37,** 2600–2616.

Fraedrich, K., and H. Böttger, 1978: A wavenumber–frequency analysis of the 500 mb geopotential at 50°N. *J. Atmos. Sci.*, **35,** 745–750.

——, and E. Kietzig, 1983: Statistical analysis and wavenumber–frequency spectra of the 500 mb geopotential along 50°S. *J. Atmos. Sci.*, **40,** 1037–1045.

Frederiksen, J. S., 1982: A unified three-dimensional instability theory of the onset of blocking and cyclogenesis. *J. Atmos. Sci.*, **39,** 969–982.

Gall, R., 1976a: A comparison of linear baroclinic instability theory with the eddy statistics of a general circulation model. *J. Atmos. Sci.*, **33,** 349–373.

——, 1976b: Structural changes of growing baroclinic waves. *J. Atmos. Sci.*, **33,** 374–390.

Grieger, N., and G. Schmitz, 1984: The Northern Hemisphere stationary planetary waves and associated Eliassen–Palm cross sections of the stratosphere and mesosphere. *Z. Meteor.*, **34,** 341–353.

Hasselmann, K. H., 1988: PIPs and POPs: The reduction of complex dynamical systems using principal interaction and oscillation patterns. *J. Geophys. Res.*, **93,** 11 015–11 021.

Hoskins, B. J., and A. J. Simmons, 1978: The life cycles of some nonlinear baroclinic waves. *J. Atmos. Sci.*, **35,** 414–432.

Lim, G. H., and J. M. Wallace, 1991: Structure and evolution of baroclinic waves as inferred from regression analysis. *J. Atmos. Sci.*, **48,** 1718–1732.

Randel, W. J., and J. L. Stanford, 1985a: An observational study of medium-scale wave dynamics in the Southern Hemisphere summer. Part I: Wave structure and energetics. *J. Atmos. Sci.*, **42,** 1172–1188.

——, and ——, 1985b: The observed life cycle of a baroclinic instability. *J. Atmos. Sci.*, **42,** 1364–1373.

Simmons, A. J., and B. J. Hoskins, 1976: Baroclinic instability on the sphere: Normal modes of the primitive and quasigeostrophic equations. *J. Atmos. Sci.*, **33,** 1454–1477.

Trenberth, K. E., and J. G. Olson, 1988: ECMWF global analyses 1979–1986: Circulation statistics and data evaluation. NCAR Tech. Note, NCAR/TN-300+STR, 94 pp. [Available from NCAR, P.O. Box 3000, Boulder, CO 80307-3000.]

Valdes, P. J., and B. J. Hoskins, 1988: Baroclinic instability of the zonally averaged flow with boundary layer damping. *J. Atmos. Sci.*, **45,** 1584–1593.

von Storch, H. H., U. Weese, and J. S. Xu, 1990: Simultaneous analysis of space–time variability: Principal oscillation patterns and principal interaction patterns with applications to the Southern Oscillation. *Z. Meteor.*, **40,** 99–103.

——, T. Bruns, I. Fischer-Bruns, and K. Hasselmann, 1988: Principal oscillation pattern analysis of the 30- to 60-day oscillation in general circulation model equatorial troposphere. *J. Geophys. Res.*, **93,** 11 022–11 036.

Xu, J.-S., 1990: Predicting the state of the Southern Oscillation using principal oscillation pattern analysis. *J. Climate,* **3,** 1316–1329.

——, 1993: The joint modes of the coupled atmosphere–ocean system observed from 1967 to 1986. *J. Climate,* **6,** 816–838.